

N89-25191

FLUTTER SUPPRESSION USING EIGENSPACE FREEDOMS TO MEET REQUIREMENTS

William M. Adams, Jr.
NASA Langley Research Center
Hampton, Virginia

Robert E. Fennell
Clemson University
Clemson, South Carolina

and

David M. Christhilf
Planning Research Corporation
Hampton, Virginia

INTRODUCTION

This paper, although much more tersely written, is similar in content to reference 1; however, additional results are presented herein.

Since the early works (refs. 2 and 3) describing the freedoms in multivariable systems beyond eigenvalue assignment, a number of researchers have expanded and applied the eigenspace design approach (e.g. refs. 1, and 4-9). The contribution of reference 1 and this paper is to provide a systematic procedure for solving for eigenspace variables such that design requirements are met. The design requirements are expressed as inequality constraints which must be satisfied by a constrained optimization procedure.

Results are presented which show an application of the procedure to the design of a control law to suppress symmetric flutter on an aeroelastic vehicle. In this example, the stability of the flutter mode is sensitive to change in dynamic pressure and eigenspace methods are used to enhance the performance properties of a "minimum energy" linear quadratic regulator (LQR) designed controller. Results indicate that the eigenspace methods coupled with order reduction can provide a low-order controller such that the closed-loop system stability is relatively insensitive to changes in dynamic pressure. However, some sacrifice of robustness with respect to error at the input occurred; this design example thus illustrates the necessity for tradeoff of conflicting requirements.

An outline of the material presented in the paper follows.

- **EIGENSPACE FREEDOMS**
- **DESIGN APPROACH**
- **PLANT DESCRIPTION**
- **STATE FEEDBACK**
- **FULL ORDER OBSERVER**
- **REDUCED ORDER CONTROLLER**

EIGENSPACE DESIGN FREEDOMS

Consider a linear time invariant system with m inputs u . For the case of a full-state controller, one can place all controllable poles, λ_i ; all eigenvectors, v_i , can be modified, including those associated with uncontrollable poles (refs. 2, 3, and 7). Each closed-loop eigenvector, v_i , must, however, lie in the subspace, W_i , that is spanned by

$$(\lambda_i I - A)^{-1} B$$

It has been assumed here that the eigenvalues are all distinct. The basis for W_i is computed using singular value decomposition techniques (refs. 10 and 11). Thus, as shown below, a designer is free to choose m variables c_i for each real eigenvalue ($2m$ variables for each complex conjugate pair of eigenvalues). When the constraint that $v_i^* v_i = 1$ is imposed, the number of free variables becomes $m-1$ for real eigenvalues ($2(m-1)$ for each complex conjugate pair of eigenvalues). Here v_i^* is the conjugate transpose of v_i .

SYSTEM

$$dx/dt = Ax + Bu$$

u is m by 1

STATE FEEDBACK

$$u = -Kx$$

FREEDOMS

$$\lambda_i$$

PLACE ALL CONTROLLABLE POLES

$$v_i$$

MODIFY ALL EIGENVECTORS

$$v_i = W_i c_i$$

c_i IS $m \times 1$ AND W_i IS BASIS FOR
 $(\lambda_i I - A)^{-1} B$

DESIGN APPROACH

Given a linear model, the design process for development of a control law to suppress symmetric flutter begins with the assumption of the availability of full-state feedback. A minimum energy stabilizing feedback design is obtained using linear quadratic regulator (LQR) theory (ref. 12). The minimum energy stabilizing solution is the solution which occurs when the performance of the controller is measured solely by the control deflection requirements (i.e., the state weighting matrix is zero)(ref 12).

The second step is to utilize a subset of the eigenvector freedoms to modify the full-state feedback design to minimize the sensitivity of the critical closed-loop pole to variation in a system parameter. This minimization is performed subject to design constraints.

The third step is to relax the full-state feedback assumption and develop a full-order observer which approximately recovers the robustness characteristics of the reduced sensitivity full-state feedback design (ref. 13). Eigenspace techniques are employed in developing the observer (refs. 6 and 7).

The eigenspace approach to observer design (refs. 6 and 7) is an alternate approach to that of reference 13. The two are equivalent in the limit in that each recovers the full-state robustness characteristics for plants with no right half plane transmission zeros. The eigenspace approach is more flexible in the sense that one can individually approach the limit for selected observer poles as opposed to the simultaneous approach of reference 13.

The final step is to reduce the full-order controller to an order that is low enough to be implementable.

—— **LQR DESIGN (MINIMUM ENERGY STABILIZING FEEDBACK)**

—— **EIGENVECTOR MODIFICATION FOR REDUCED SENSITIVITY
(FULL-STATE FEEDBACK)**

—— **OBSERVER DESIGN FOR LOOP TRANSFER RECOVERY (FULL-
ORDER OBSERVER)**

—— **CONTROLLER ORDER REDUCTION**

EIGENSPACE TECHNIQUES TO MEET REQUIREMENTS

The method is to choose a subset of the closed-loop eigenvectors to be modified and then to determine values for each selected vector c_j such that a function of these variables is minimized. In this study the magnitude of the sensitivity of the flutter mode eigenvalue to variations in dynamic pressure is minimized subject to n_g constraints. In the equations below g_{uj} and g_{lj} are upper and lower bounds, respectively, on the j th constrained

variable g_j (e.g. control saturation). The scalar variable, $\bar{g}_j \geq 0$, is the violation of the j th constraint. The vector u_j is a left eigenvector of the system matrix A .

The constrained optimization process appends a weighted square of each constraint violation, \bar{g}_j , to the function to be minimized (P is a positive definite diagonal weighting matrix). In the limit as each weight P_{jj} approaches infinity, $|S|^2$ is minimized subject to the constraints provided that the number of constraints on a constraint boundary in this limit is less than the number of design variables (ref. 14). A nongradient optimizer was employed in this study (ref. 15).

The constraints to be employed in this study are on root mean square (rms) values for control deflections, control rates, and incremental wing root bending moment, shear, and torque due to random gust inputs. In addition a constraint was imposed upon robustness of the control law with respect to error at the plant input.

— PARAMETERIZATION OF ATTAINABLE EIGENVECTORS

$$v_j = W_j c_j, j = 1, n$$

— SENSITIVITY

$$S = d\lambda_i / dq = \frac{u_i^* (dA/dq) v_i}{u_i^* v_i}$$

— CONSTRAINTS

$$\bar{g}_j = \max(0, g_j - g_{uj}, g_{lj} - g_j), j=1, n_g$$

— AUGMENTED PERFORMANCE INDEX

$$J_p = |S|^2 + \bar{g}^T P \bar{g}$$

— NONGRADIENT OPTIMIZATION

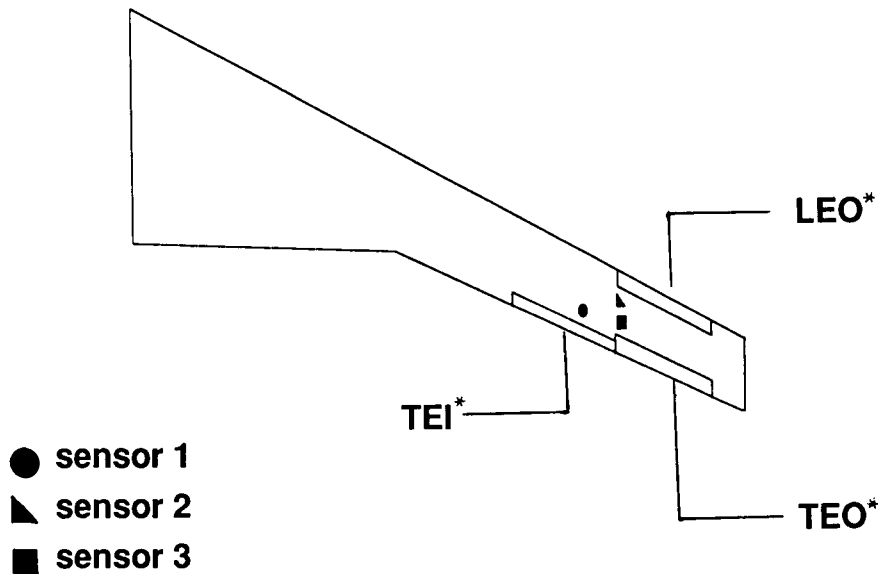
CONTROL SURFACE AND SENSOR LOCATIONS
(Symmetric Full Span)

The mathematical model is based upon one that represents an actual aeroelastic drone vehicle (ref. 16). The actual vehicle has only one effective control surface for flutter suppression (the trailing-edge outboard surface shown in the planform view). For this study fictitious leading-edge and inboard trailing-edge controls have been added per semispan to provide three effective symmetric and antisymmetric flutter suppression surfaces. The surfaces are driven by high bandwidth actuators each having transfer functions

$$\delta_i = \frac{180 (314)^2}{(s + 180) (s^2 + 251s + (314)^2)} \delta_{c_i}$$

where δ_{c_i} is commanded deflection and δ_i is actual. The poles for each actuator are separated slightly in the mathematical representation to improve numerical conditioning.

Three vertical accelerometers are located as indicated. These high bandwidth devices have virtually no dynamics in the frequency range of interest and are, therefore, modeled as unity gains. The sensor locations correspond to three of the four sensors on the actual wing. The locations were chosen early in the wing design cycle as desirable for flutter suppression sensors based upon analytical studies (ref. 17).



*Trailing-edge inboard (TEI); leading-edge inboard (LEI); trailing-edge outboard (TEO).

DESIGN MODEL
(Symmetric Modes)

The aircraft is designed to be symmetric about a plane perpendicular to the wings and to intersect them at the centerline. Consequently, to a good approximation for small perturbations from rectilinear flight, the symmetric and antisymmetric degrees of freedom are uncoupled. Thus, symmetric and antisymmetric designs can be obtained separately. This study considers symmetric modes only.

The underlying symmetric evaluation model contains 2 rigid body and 11 elastic modes. A lower-order linear time invariant state space design model was extracted from the evaluation model. The design model was chosen by a trial and error truncation of modes. The effect of a candidate truncation upon frequency responses of interest and upon the loci of eigenvalues with dynamic pressure was observed. Modes having little impact were deleted. The modes deleted included the rigid-body modes, predominantly fuselage and tail modes and higher-order wing modes. If they are troublesome, rigid-body contributions to the actual sensor (accelerometer) outputs can be removed either by employing a high pass filter or by making use of measured linear and angular accelerations at the center of mass.

The resulting design model is twenty-sixth order. The uncontrollable gust states correspond to a Dryden filter representation with a gust scale length of 2500 ft. The rational function approximation (ref. 18) made to the unsteady aerodynamic forces included one lag term having a reduced frequency of 0.13. The B matrix is independent of the dynamic pressure, q. The u vector contains the three commanded control deflections and a white noise input into the Dryden filter.

$$\dot{x} = A(q)x + Bu$$

$$y = C(q)x$$

5 MODES (SECOND ORDER)	10
1 AERO LAG PER MODE	5
3 THIRD-ORDER ACTUATORS	9
2ND ORDER GUST	2

26 STATES

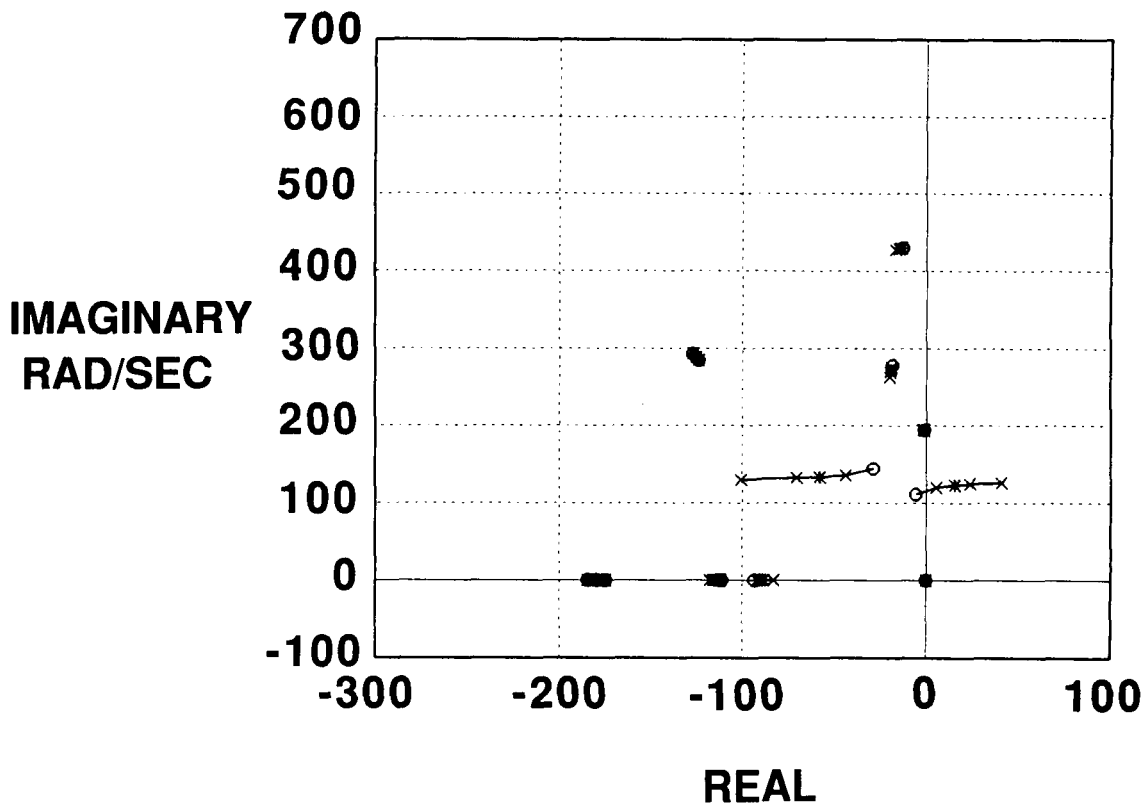
DYNAMIC PRESSURE ROOT LOCUS
(Uncontrolled Plant)

A variation of the uncontrolled design model roots with dynamic pressure is shown. The variation corresponds to an altitude variation at a fixed Mach number of 0.775. With no feedback, the actuator poles are stationary near (-180, 0) and (-120, ±280).

The circle symbol corresponds to the lowest dynamic pressure. The highest dynamic pressure point corresponds to a dynamic pressure 44 percent above that at flutter. The 44 percent increase in flutter dynamic pressure corresponds to what would be required if active controls were to provide the full 20 percent margin above the design dive speed for a transport aircraft.

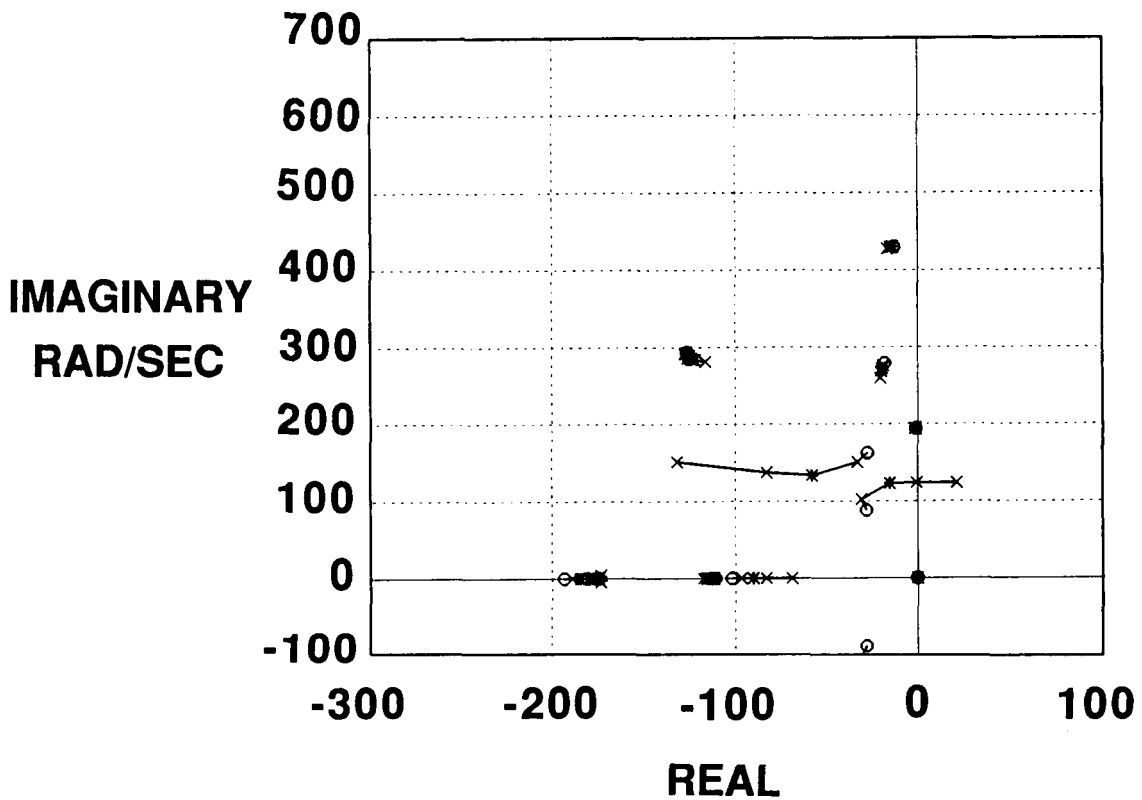
The flutter is explosive (i.e., the time to double amplitude decreases rapidly with increasing dynamic pressure). The interacting modes exhibit classical frequency coalescence. The zero dynamic pressure characteristics of the retained elastic modes in ascending frequency order are 1) wing bending, 2) second wing bending with some torsion, 3) wing fore and aft bending with a torsional normal component, 4) wing torsion, and 5) a higher order wing mode exhibiting bending and torsion.

The * on the figure depicts the point for which the controller was designed. This design point is approximately 11.5 percent above the uncontrolled flutter dynamic pressure.



DYNAMIC PRESSURE ROOT LOCUS
(Min Energy LQR Controller)

The locus of closed-loop roots with dynamic pressure for the minimum energy Linear Quadratic Regulator (LQR) full-state feedback controller shows that the closed-loop system remains stable only up to a point 20 percent above that of open-loop flutter (7.7 percent above the design point). One could maximize robustness with respect to error at the input by repeating the LQR design at each dynamic pressure and scheduling the controller as a function of dynamic pressure; however, it is of interest here to see what tradeoffs are required to minimize the effect of dynamic pressure on the closed-loop stability characteristics.



DESIGN CONSTRAINTS

The constraints to be imposed on the reduced sensitivity full-state feedback design will now be enumerated. The first two sets of constraints were that the rms control deflections and rates not exceed 5 deg and 372 deg/sec, respectively, when the system was forced by a vertical gust field having a 12 ft/sec rms gust velocity. The physical control limits were ± 15 deg and ± 740 deg/sec. Bending moment, shear, and torque rms incremental loads at the wing root were also constrained to remain near their values at a stable point (lowest dynamic pressure point on the previous root locus). Finally, the minimum singular value of the return difference matrix was constrained to be

$$\sigma_{\min} = \min_{\omega} \sigma(I + K(j\omega)G(j\omega)) > 0.6$$

where $G(s)$ is the plant transfer matrix and $K(s)$ is the controller transfer matrix. This singular value is a measure of robustness due to multiplicative error at the input. Error occurrences at other points are important but are not addressed herein. The choice of $\sigma_{\min} > 0.6$ allows an appreciable tradeoff to occur between σ_{\min} and the sensitivity reduction objective. It is also representative of robustness levels that have been achieved in implementable designs (e.g. ref. 19).

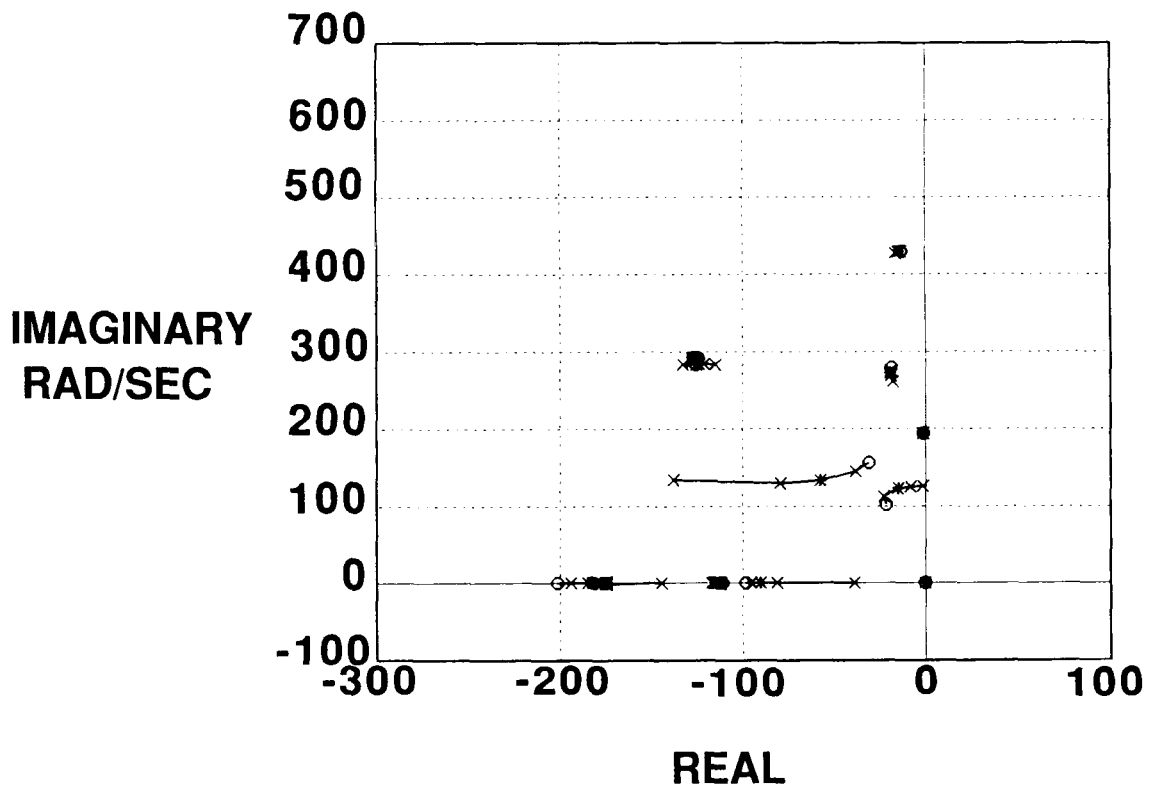
A value for $\sigma(j\omega)$, the minimum singular value at the frequency ω , near zero means that the nominal closed-loop system is near instability at that frequency. Thus, even a small difference between the true plant and its nominal representation can cause instability. For the minimum energy linear quadratic regulator (LQR) full-state feedback design of this paper $\sigma(j\omega) = \bar{\sigma}(j\omega) = \sigma_{\min} = 1$ at all frequencies. (Here $\bar{\sigma}(j\omega)$ is the maximum singular value at the frequency ω .) This fact can be seen by examining the development of the Kalman inequality (e.g. ref. 20, p. 7-3). When the state weightings are null (minimum energy controller) and the control weightings are unity, the equality holds.

	RMS CONTROL DEFLECTION DEGREES	RMS CONTROL RATE DEGREES/SEC	RMS BENDING MOMENT in-lb	RMS SHEAR lb	RMS TORQUE in-lb	MINIMUM SING. VALUE
UPPER BOUND	5	372	30,000	1,000	2,000	1.
LOWER BOUND	0	0	0	0	0	.6

RMS GUST VELOCITY 12 FT/SEC

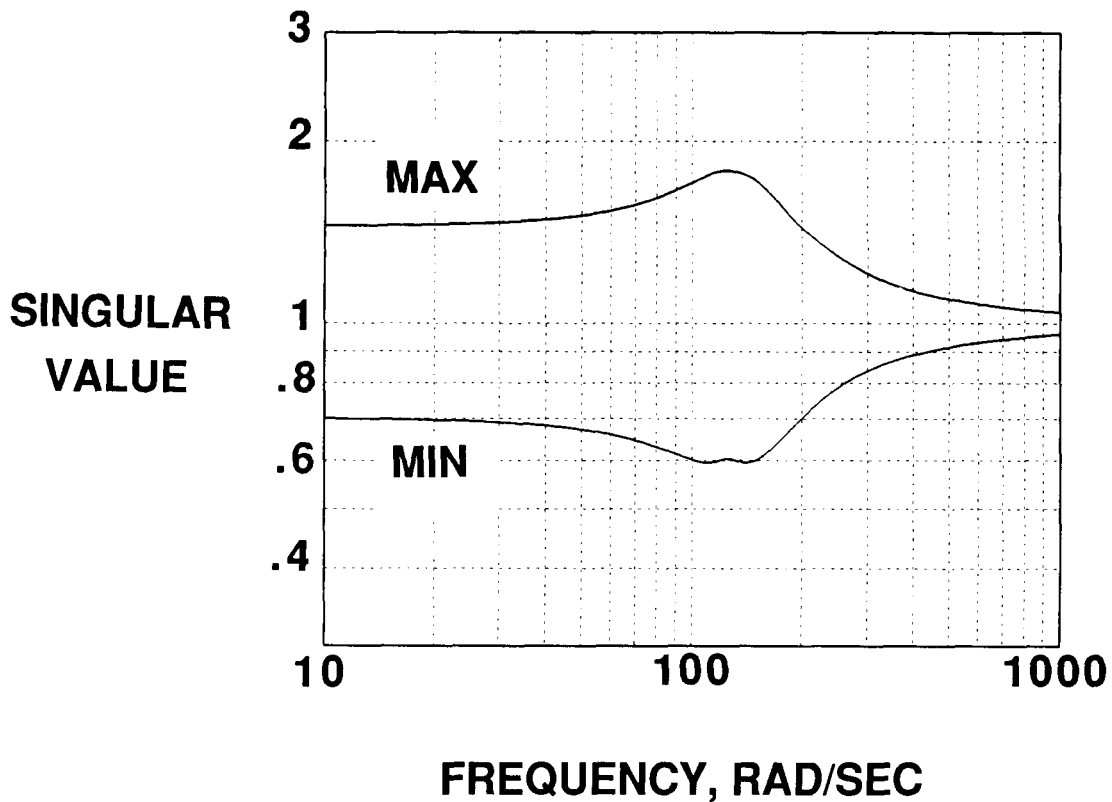
DYNAMIC PRESSURE ROOT LOCUS
(Reduced-Sensitivity Full-State Feedback)

A full-state feedback design was obtained for which the critical eigenvalue had reduced sensitivity to dynamic pressure variation. This design satisfied the constraints at the design point. The design was achieved by utilizing the eigenvector freedoms associated with the two coalescent modes. Thus, there were 12 free variables (eight after mode normalization constraints). The resulting control law stabilizes the system over the full range of dynamic pressures.



SINGULAR VALUES OF $(I + K(s)G(s))$
(Reduced-Sensitivity Full-State Feedback)

The locus of maximum and minimum singular values of the return difference for the reduced sensitivity state feedback controller shows the constraint of 0.6 was met as prescribed. The figure illustrates the tradeoff that has occurred. (for comparison, as discussed earlier, the minimum energy LQR controller with unity control weightings has a minimum (and maximum) singular value of one at all frequencies). Further analysis is required to assess how conservative the unstructured singular values are; nevertheless, a minimum value of 0.6 indicates a substantial capability for rejection of input disturbances.



OBSERVER DESIGN

Eigenspace techniques were also employed to obtain a full-order observer. The approach was to place observer poles near the finite plant transmission zeros and the corresponding observer eigenvectors at plant left zero directions (refs. 6 and 7). Poles in excess of the transmission zeros were placed far into the left half plane with arbitrary eigenvectors. The observer poles corresponding to the six transmission zeros at zero (from the three sensors being accelerometers) were displaced an arbitrary five units into the left half plane to avoid problems associated with implementation of pure integrators. In the equations H is the observer gain matrix, K_m is the reduced-sensitivity full-state feedback gain matrix and the subscript "o" emphasizes that the controller is developed for the design point but then evaluated at off-design points.

SYSTEM MODEL

$$\dot{x} = Ax + Bu$$

$$y = Cx$$

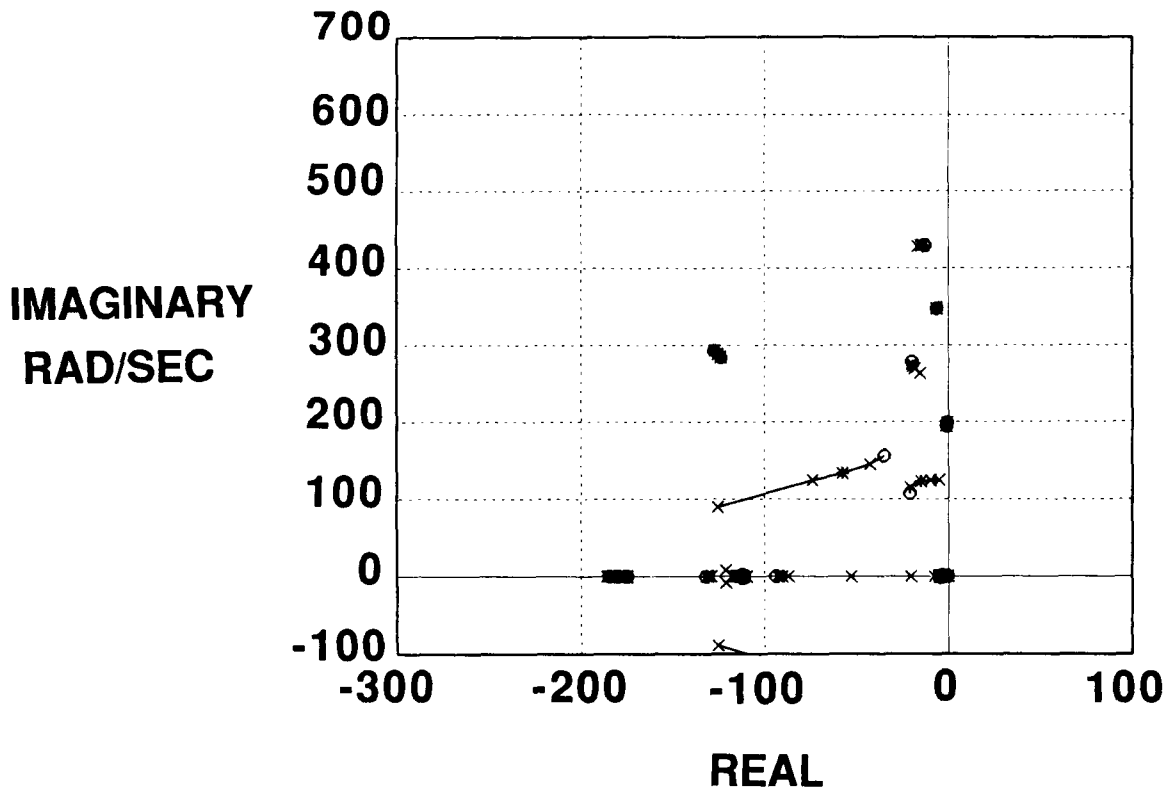
CONTROLLER

$$\dot{z} = Hy + (A_o - B_o K_M - H C_o) z$$

$$u = -K_M z$$

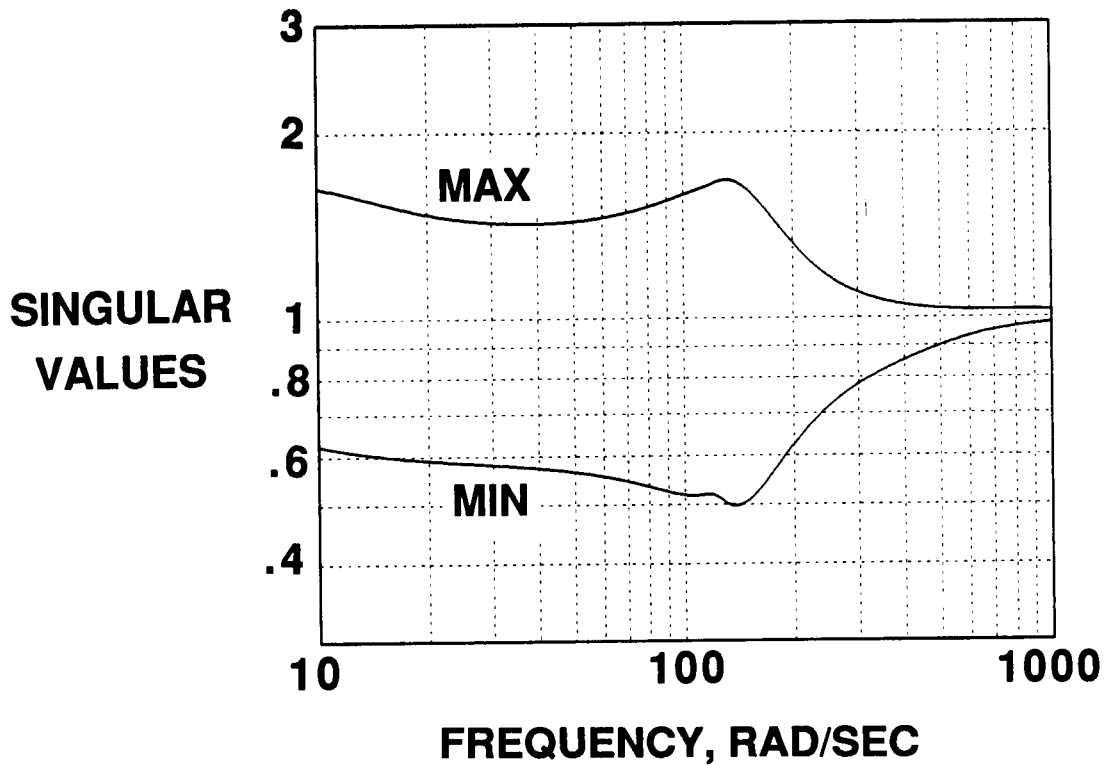
DYNAMIC PRESSURE ROOT LOCUS
(Reduced-Sensitivity Feedback Plus Full-Order Observer)

The locus of poles with dynamic pressure for reduced-sensitivity full-state feedback plus a full-order observer to estimate the states given only three accelerometer outputs shows that stability was also achieved for this case over the full dynamic pressure range. One can see by comparing this figure with the corresponding one for reduced-sensitivity full-state feedback that controller poles are located near $(-5, 0)$ rad/sec, $(-130, 0)$ rad/sec, a lightly damped complex conjugate pair near a frequency of 200 rad/sec and a complex conjugate pair near a frequency of 340 rad/sec. If the true plant pole/zero pair near 200 rad/sec is different than that of the design model, the closed-loop performance in this frequency region may be substantially degraded. Further discussion of this point is given below in the section describing the reduced-order controller performance with respect to the evaluation model of the plant. Other poles not shown here are further in the left half plane than the limits of the figure. A compilation of the full set of observer poles at the design point and a locus of all closed-loop poles with dynamic pressure are given in reference 1.



SINGULAR VALUES OF $(I + K(s)G(s))$
(Reduced-Sensitivity Feedback Plus Full-Order Observer)

A small degradation in minimum singular value resulted from adding the observer to estimate the states. The minimum singular value in this case is about 0.5 as compared with 0.6 in the reduced-sensitivity full-state feedback case.



CONTROLLER ORDER REDUCTION

The full-order controller was then reduced from 26th order down to eighth order. The process employed in the reduction was to determine which controller states had little impact upon controller performance. The controller was transformed to modal form, modes were truncated based upon small residues and/or large separation from the flutter frequency, and the resulting closed-loop root locus and minimum singular value of the return difference matrix were examined; this allowed determination of the highest frequency controller mode that should be retained. Relatively unimportant modes having eigenvalues with amplitudes greater than the highest frequency mode to be retained were temporarily included in the controller representation. The input and output controller matrices were balanced and a second modal decomposition was performed. The temporarily included modes were then removed by residualization. For this case nine states were removed by truncation and nine states were removed by residualization.

The resulting eighth-order controller has six poles clustered near $(-5, 0)$ rad/sec and one complex conjugate pair near a frequency of 200 rad/sec.

TRUNCATION

MODAL DECOMPOSITION

TRUNCATE MODES WITH SMALL EFFECT ON CONTROL

RESIDUALIZATION

BALANCED REALIZATION

RESIDUALIZED FAST MODES

REDUCED ORDER CONTROLLER

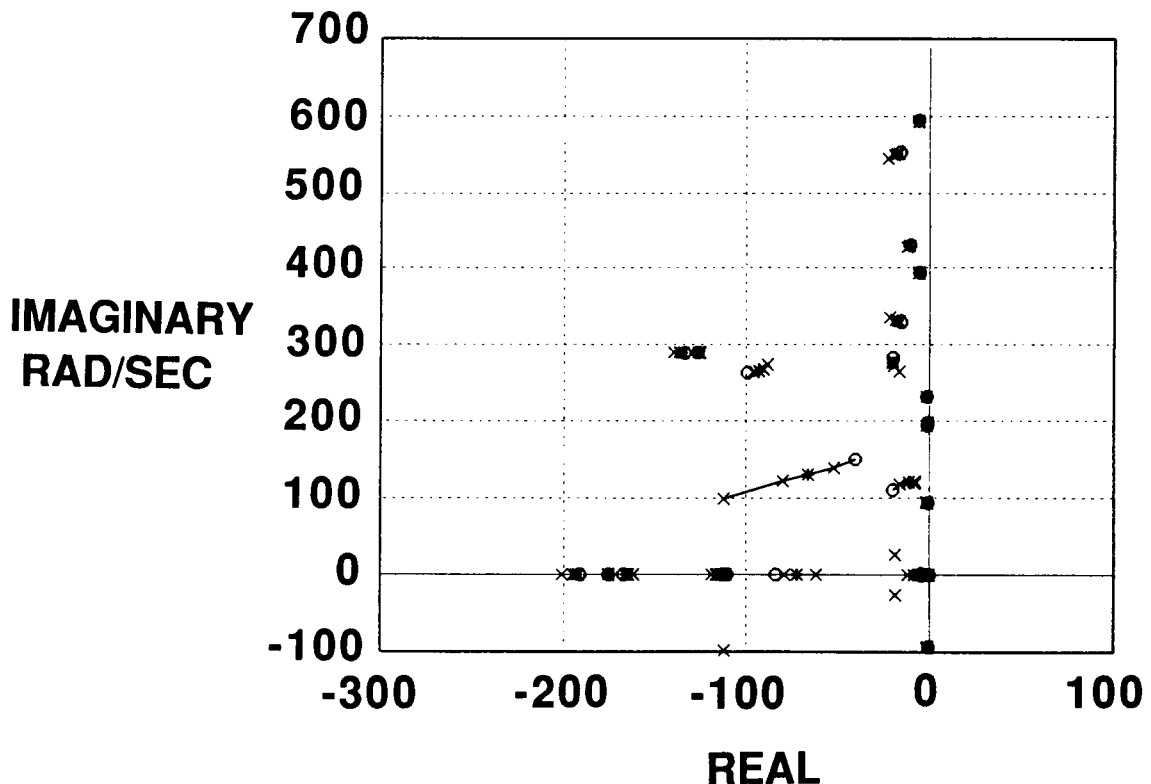
EIGHTH ORDER

DYNAMIC PRESSURE ROOT LOCUS
(Evaluation Plant with Reduced Order Controller)

This figure shows that stability is achieved over the full dynamic pressure range with an eighth-order controller. In fact, the sensitivity of the critical closed-loop pole to dynamic pressure is lower for this controller and the evaluation model of the plant than was found for the design model with reduced sensitivity full-state feedback. The retained controller poles were the six poles near $(-5, 0)$ rad/sec, and a very lightly damped complex conjugate pair of poles at a frequency near 200 rad/sec.

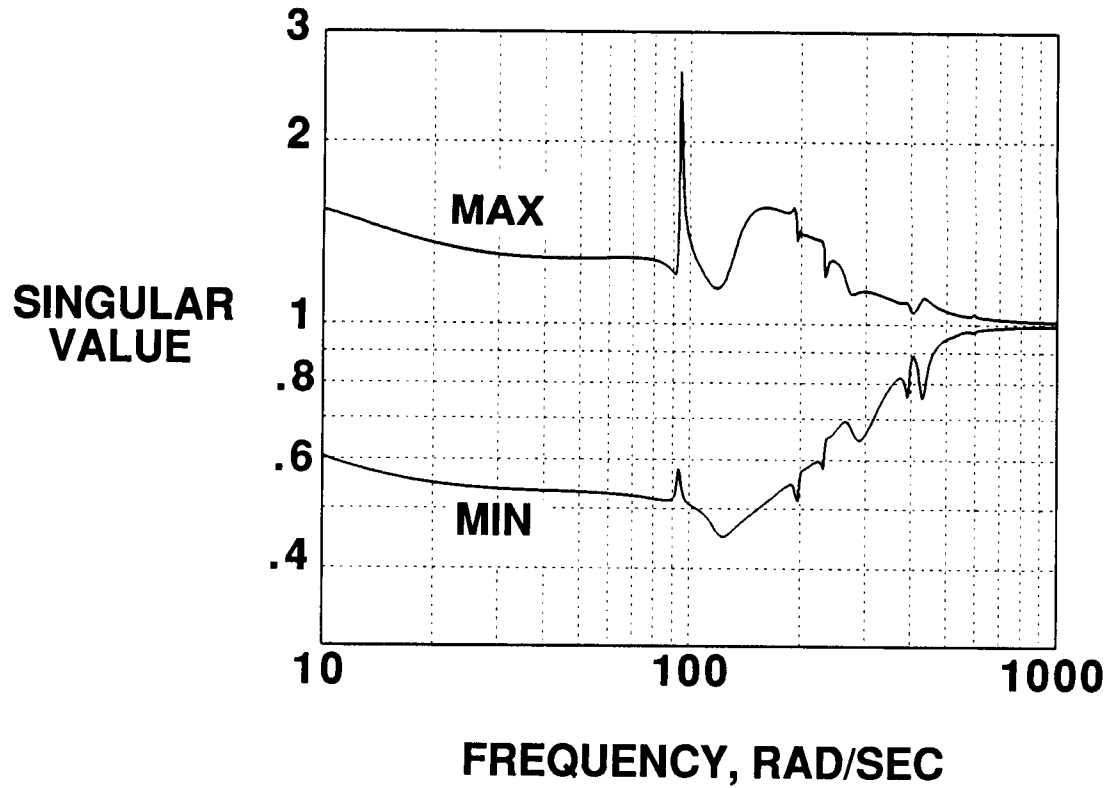
The latter controller poles which have associated zeros near but to the left of them in the left half plane are troublesome since they and the corresponding plant poles are severely underdamped. From a stability standpoint these controller poles can be removed for the nominal system; however, the singular value measure of robustness is then degraded substantially at this frequency. For this particular vehicle, one can argue for two reasons that the problem is not real but arises only due to a plant modeling deficiency.

The first reason is that the vehicle has been wind tunnel tested with no problems occurring in this frequency range. The second reason is that the plant mode at this frequency is predominantly fore and aft bending with a small amplitude torsional component. The doublet lattice aerodynamic computation produces no aerodynamic damping due to the fore and aft motion. Thus, the mode should probably be further in the left half plane than is the case for the mathematical model. In general, however, one would prefer to gain stabilize or perhaps notch out a high-frequency underdamped pole that remains essentially stationary.



SINGULAR VALUES OF $(I + K(s)G(s))$
(Evaluation Plant Model with Reduced Order Controller)

The minimum singular value of the return difference matrix for the eighth-order controller and the evaluation model of the plant is about 0.44 as compared with 0.5 for the full-order controller and the design model. This is a guaranteed margin and may be quite conservative. The spike seen at a frequency of 92 rad/sec is due to a mode in the evaluation model that was not accounted for in the design. The mode is a predominantly fuselage mode that remains unchanged in frequency over the dynamic pressure range. It could be dealt with effectively with a notch filter.



RMS PERFORMANCE
(LQR and RSFSF)

All of these results are for a Dryden gust spectrum with rms gust input of 12 ft/sec. The rms control power performances for LQR at the design point are on the order of 10 to 25 percent of the constraint.

For the reduced-sensitivity full-state feedback (RSFSF) design, i.e., the eigenspace reduced sensitivity design, the rms control effort at the design point varies from approximately 100 to 225 percent larger than for LQR for each of the outboard surfaces. Lower usage is made of the smaller, less effective, inboard trailing-edge control surface. An increase in rms output with increasing dynamic pressure is evident; the sharper increase between the last two points is due to the larger dynamic pressure difference here than for other pairs of points and, more importantly, to the low damping in the critical pole at the highest dynamic pressure condition. Small constraint violations occur at the highest dynamic pressure.

		Dynamic Pressure, lb/in ²					design point
RMS			4.417	4.768	5.141	5.537	6.639
LQR	δ , deg	TEO	.480	.475	.571	2.07	---
		TEI	.542	.460	.494	1.62	
		LEO	.899	.768	.831	2.74	
	$\dot{\delta}$, deg/sec	TEO	49.9	56.6	71.3	248.3	
		TEI	41.5	46.5	57.8	199	---
		LEO	70.1	78.5	97.7	336	
	M, in-lb	Moment	24,337	25,727	27,146	29,969	
	S, lb	Shear	455.5	479.8	505.1	582.4	---
	T, in-lb	Torque	464.8	576	823.4	3,470.8	
RSFSF	δ , deg	TEO	1.45	1.20	1.11	1.47	6.11
		TEI	.220	.205	.215	.261	.689
		LEO	1.98	1.60	1.42	1.72	6.28
	$\dot{\delta}$, deg/sec	TEO	158.5	164.1	174.5	196.6	438.8
		TEI	22.7	24.5	27.4	32.5	72.3
		LEO	163.5	165.5	171.2	186.9	400.5
	M, in-lb	Moment	24,158	25,479	27,042	29,010	39,587
	S, lb	Shear	440.2	468.3	501.1	541.6	748.3
	T, in-lb	Torque	352.5	414.9	542.7	779.0	2,647

CONSTRAINTS: $\delta_{rms} < 5$ deg, $\dot{\delta}_{rms} < 372$ deg/sec

$M_{rms} < 30K$ in-lb

$S_{rms} < 1000$ lb, $T_{rms} < 2000$ in-lb

RMS PERFORMANCE
(FOC and FOM/ROC)

For the full-order controller (FOC) the utilization of the TEI control is further reduced as compared to the RSFSF results on the previous page. The TEO rms deflection is approximately quadrupled as compared with RSFSF except at the highest dynamic pressure; the LEO control deflection is also increased except at the highest dynamic pressure where it is reduced by over 30 percent. The rms rates are somewhat reduced as compared to RSFSF for the LEO surface. Wing root torque is higher at lower dynamic pressure and lower at the highest dynamic pressure as compared to the RSFSF results. No constraint violation occurs for control rate but the TEO deflection constraint is violated at the two higher dynamic pressures.

More violations occur when the eighth-order controller is coupled with the evaluation model of the plant (FOM/ROC). Little of the increased activity is due to controller reduction; this was found by comparing the design model full-order controller results (FOC) with the design model reduced order control results (not shown here). The increased activity of the FOM/ROC as compared with the FOC is primarily a result of contributions to the output from the modes in the evaluation model that were absent in the design model. For the FOM/ROC case, rate violation occurs only for the TEO control at the highest dynamic pressure. The rms deflection violations are small except for TEO at the highest dynamic pressure.

Load rms violations are also small except at the highest dynamic pressure. The loads computations are only approximate for the FOM case because modal load coefficients were only available for the five modes retained in the design model.

		Dynamic Pressure, lb/in ²					
		design point					
RMS		4.417	4.768	5.141	5.537	6.639	
FOC	δ, deg	TEO	4.04	4.38	4.78	5.29	7.41
		TEI	.141	.156	.176	.202	.269
		LEO	2.37	2.54	2.75	3.01	4.07
	δ̇, deg/sec	TEO	144.5	160.1	181.2	208.4	302.8
		TEI	17.1	18.9	21.2	24.1	28.9
		LEO	96.0	104.9	116.7	132.7	286.5
	M, in-lb	Moment	25,129	26,259	27,475	28,648	32,277
	S, lb	Shear	465	488.7	513.6	540.1	619.5
	T, in-lb	Torque	827.3	970.9	1,150	1,375	2,300
FOM/ROC	δ, deg	TEO	4.72	5.21	5.84	6.66	11.05
		TEI	.162	.183	.210	.243	.343
		LEO	2.66	2.91	3.21	3.62	5.74
	δ̇, deg/sec	TEO	181.3	203	231.9	270.3	416.1
		TEI	19.8	22	24.6	27.44	28.35
		LEO	106.4	118	133.8	154.8	225.29
	M, in-lb	Moment	27,363	28,774	30,277	31,924	38,013
	S, lb	Shear	503.8	533	564.4	599.2	728.9
	T, in-lb	Torque	962	1,155	1,398	1,718.9	3,423.3

CONSTRAINTS: $\delta_{rms} < 5$ deg, $\dot{\delta}_{rms} < 372$ deg/sec

$M_{rms} < 30K$ in-lb

$S_{rms} < 1000$ lb, $T_{rms} < 2000$ in-lb

SUMMARY

A constrained optimization methodology has been developed which allows specific use of eigensystem freedoms to meet design requirements. A subset of the available eigenvector freedoms was employed. The eigenvector freedoms associated with a particular closed-loop eigenvalue are coefficients of basis vectors which span the subspace in which that closed-loop vector must lie. Design requirements are included as a vector of inequality constraints.

The procedure was successfully applied to develop an unscheduled controller which stabilizes symmetric flutter of an aeroelastic vehicle to a dynamic pressure 44 percent above the open-loop flutter point. Eigenvector freedoms, for fixed eigenvalue locations, of the two coalescent modes were employed to minimize the sensitivity of the critical closed-loop eigenvalue to dynamic pressure variation subject to control power, loads, and robustness constraints. The reduced sensitivity was achieved at the expense of reduced robustness to errors at the input.

The design process proceeded from full-state feedback to the inclusion of a full-order observer to the selection of an eighth-order controller which preserved the full-state sensitivity characteristics.

Only a subset of the design freedoms was utilized (i.e., assuming full-state feedback only four out of 26 eigenvectors were used, and no variations were made in the closed-loop eigenvalues). Utilization of additional eigensystem freedoms could further improve the controller.

- **CONSTRAINED OPTIMIZATION METHODOLOGY DEVELOPED TO USE EIGENSYSTEM FREEDOMS TO MEET REQUIREMENTS**
- **SUCCESSFULLY USED EIGENVECTOR FREEDOMS TO LOWER SENSITIVITY TO DYNAMIC PRESSURE VARIATION**
- **REDUCED SENSITIVITY TO DYNAMIC PRESSURE ACHIEVED AT EXPENSE OF ROBUSTNESS AS MEASURED BY MINIMUM SINGULAR VALUE OF RETURN DIFFERENCE MATRIX**
- **EIGHTH ORDER CONTROLLER FOUND WHICH PRESERVED REDUCED SENSITIVITY CHARACTERISTICS**
- **UNUSED EIGENSPACE FREEDOMS COULD FURTHER IMPROVE CONTROLLER**

REFERENCES

1. Fennell, Robert E.; Adams, William M., Jr.; and Christhilf, David M.: An Application of Eigenspace Methods to Symmetric Flutter Suppression. AIAA Paper No. 88-4099-CP.
2. Moore, B. C.: On the Flexibility Offered by State Feedback in Multivariable Systems Beyond Closed-Loop Eigenvalue Assignment. IEEE Trans. Automatic Control, vol. AC-21, 1976, pp. 689-692.
3. Srinathkumar, S.: Eigenvalue/Eigenvector Assignment Using Output Feedback. IEEE Trans. Automatic Control, vol. AC-23, 1978, pp. 79-81.
4. Andry, A. N.; Shapiro, E. Y.; and Chung, J. C.: Eigenstructure Assignment for Linear Systems. IEEE Trans. Aerospace and Electronic Systems, vol. AES-19, 1983, pp. 711-729.
5. Kautsky, J.; Nichols, N. K.; and Van Dooren, P.: Robust Pole Assignment in Linear State Feedback. Int. Journal of Control, vol. 5, 1985, pp. 1129-1155.
6. Kazerooni, H.; and Houpt, P. K.: On the Loop Transfer Recovery. Int. Journal of Control, vol. 43, 1986, pp. 981-996.
7. Garrard, W. L.; Liebst, B. S.; and Farm, J. A.: Eigenspace Techniques for Active Flutter Suppression. NASA CR-4071, 1987.
8. Sobel, K. M.; and Shapiro, E. Y.: Application of Eigenstructure Assignment to Flight Control Design: Some Extensions. Journal of Guidance, Control, and Dynamics, vol. 10, 1987, pp. 73-81.
9. Klema, V.; and Laub, A. J.: The Singular Value Decomposition: Its Computation and Some Applications. IEEE Trans. Automatic Control, vol. AC-25, 1980, pp. 164-176.
10. Porter, B.; and D'Azzo, J. J.: Algorithm for Closed-Loop Eigenstructure Assignment by State Feedback in Multivariable Linear Systems. Int. Journal of Control, vol. 27, 1978, pp. 943-947.
11. Golub, G. H.; and Van Loan, C. F.: Matrix Computations. The Johns Hopkins University Press, Baltimore, Maryland. 1983.
12. Kwakernaak, H.; and Sivan, R.: Linear Optimal Control Systems. Wiley Interscience, New York. 1972.
13. Doyle, J. C.; and Stein, G.: Multivariable Feedback Design: Concepts for a Classical/Modern Synthesis. IEEE Trans. on Automatic Control, vol. AC-26, 1981, pp. 4-16.
14. Courant, R.: Variational Methods for the Solution of Problems of Equilibrium and Vibrations. Bull. American Math Society, vol. 49, January 1943, pp. 1-23.
15. Olsson, D. M.; and Nelson, L. S.: The Nelder-Mead Simplex Procedure for Function Minimization. Technometrics, vol. 17, 1975.
16. Murrow, H. N.; and Eckstrom, C. V.: Drones for Aerodynamic and Structural Testing (DAST) - A Status Report. AIAA Paper No. 78-1485. Presented at the 1978 Atmospheric Flight Mechanics Conference, August 1978.

17. Boeing Wichita Company: Integrated Design of a High Aspect Ratio Research Wing with an Active Control System for Flight Tests on a BQM-34E/C Drone Vehicle. NASA CR-166108, 1979.
18. Rodger, Kenneth L.: Airplane Math Modeling Methods for Active Control Design. AGARD CR-228, August 1977.
19. Adams, William M., Jr.; and Tiffany, Sherwood H.: Design of a Candidate Flutter Suppression Control Law for the DAST ARW-2. NASA TM-86257, July 1984.
20. Ridgely, D. Brett; and Banda, Siva S.: Introduction to Robust Multivariable Control. AFWAL-TR-85-3102, February 1986.